Article:
Bawazer, LA, Ihli, J, Levenstein, MA et al. (2018) Enzymatically-Controlled Biomimetic Synthesis of Titania/Protein Hybrid Thin films. Journal of Materials Chemistry B, 6. pp. 3979-3988. ISSN: 2050-750X

https://doi.org/10.1039/C8TB00381E

Enzymatically-Controlled Biomimetic Synthesis of Titania/Protein Hybrid Thin films

L. A. Bawazer[a*], J. Ihli[a*], M. A. Levenstein[a,b], L. J. C. Jeuken[c] and F. C. Meldrum[a], D. G. G. McMillan[c,d†*]

[a.] *School of Chemistry, University of Leeds, Woodhouse Lane, Leeds, LS2 9JT, United Kingdom*
[b.] *School of Mechanical Engineering, University of Leeds, Woodhouse Lane, Leeds, LS2 9JT, United Kingdom*
[c.] *School of Biomedical Sciences, University of Leeds, Woodhouse Lane, Leeds, LS2 9JT, United Kingdom*
[d.] *Department of Biotechnology, Delft University of Technology, 2629 HZ Delft, The Netherlands*

† Correspondence should be addressed to D. McMillan Email: D.G.G.McMillan@tudelft.nl

*these authors contributed equally

Although it is widely recognised that enzymes play a significant role in sculpting complex silica skeletons in marine sponges, the potential for exploiting enzymes in materials synthesis has not yet been fully harnessed. In this work we show that the digestive enzyme papain can self-assemble into monolayers on oxide surfaces, where they then drive the formation of crystalline titanium dioxide nanoparticles. This dual functionality of thin film formation and mineralization promotion has the potential to enable the construction of hierarchical inorganic/organic structures in the form of continuous amorphous titania/protein films which can be refined to 93% anatase post annealing. Additional control over the film thickness is afforded by layer-by-layer processing using a simple dip-coating approach. Papain's TiO_2-mineralizing activity displays complex kinetics that deviates from the native Michaelis-Menten kinetic activity, yet deactivation studies demonstrate that this activity relies upon residues that are essential for catalytic site function. These parameters provide unique insight into enzymatic biomineralization, allowing a flexible route to achieving bioengineered titania heterostructures, and potentially providing a green-chemistry solution to photovoltaic cell development

Introduction

Inorganic and hybrid organic-inorganic thin films are fundamental to a huge range of applications, including microelectronics,[1] water treatment,[2] photovoltaics,[3] protective barrier coatings,[4] and chemical and biological sensors.[5] Methods of thin film synthesis are similarly diverse, ranging from low-temperature solution-processing techniques such as layer-by-layer dip-coating,[6] to high-temperature techniques including thermal oxidation and chemical vapor deposition.[7] While low-temperature approaches are advantageous due to their lower cost and processing ease, many solid-state thin film materials are currently only accessible through energy-intensive routes involving high

vacuum or high temperature, or through the use of toxic reagents.[8,9] There is therefore tremendous potential for the development of approaches that can generate functional thin films from high performance materials under ambient conditions.

The observation that natural biomineralization processes operate in aqueous solutions and low temperatures to form hierarchically organized inorganic/ organic composites with superior physical properties demonstrates the feasibility of this goal.[10-12] Indeed, the structural and chemical diversity of biominerals indicates that the biogenic control strategies employed can be readily tailored to the formation of a wide range of materials.[13-15] A range of biomimetic approaches have been explored to direct the formation of inorganic crystals and glasses from aqueous solution,[16-18] where the use of soluble organic additives has received the most attention. Biomolecules including small molecules,[19,20], short polypeptides,[21] adhesive proteins,[22], and carbohydrates[23] have all been shown to be active in controlling mineralization processes, enabling, for example, synthesis of patterned assemblies of inorganic nanoparticles,[20] , and mineralization under conditions where it does not typically occur.[14,19] There are also few examples of the use of enzymes in controlling mineralization processes, where the best example is arguably provided by the enzyme silicatein.[18,24] In addition to being active *in vivo* in generating the silica elements in marine sponges, this enzyme can also be employed in synthetic environments to generate nanoparticles of anatase-TiO_2[25] and quartz-like silicates[15] under solution conditions that would not otherwise support the formation of crystalline products.

Despite this powerful example, the potential for exploiting enzymes to control mineralization has received relatively little attention. This opportunity gap exists because enzymes can be challenging to work with outside their native cellular physiology,[26] and relatively few additional biomineralizing enzymes have been identified in natural systems.[10,27,28] Some digestive proteases, such as papain and trypsin, which are straightforward to work with, and are related to natural biomineralizing enzymes, have shown potential for mineralizing oxide nanoparticles *in vitro*.[29] However, the possibility of using mineralizing enzymes to control the formation of complex structures – as occurs in biological systems – has not yet been explored. In this work we demonstrate that the enzyme papain can self-assemble into monolayers on oxide surfaces, while still retaining its ability to catalyze mineralization processes. This dual behavior can then be exploited to produce hybrid inorganic/ organic thin films *via* simple layer-by-layer processing, where the papain monolayers first enzymatically hydrolyze the water-soluble organo-metallic precursor titanium bis-lactatodihydroxide (TiBALDH) and then serve as a deposition surface. The resulting thin films contain TiO_2 nanoparticles, together with hydrolyzed lactate species as an organic fraction. Kinetic parameters and active site inhibition obtained for papain-driven titania mineralization in bulk solution substantiate the proposed mechanism for thin film

mineralization. Overall, these results suggest that enzymes can provide an effective biomolecular tool for producing inorganic thin-films with tunable thickness at low temperature.

Results

TiO_2/Papain Thin Film Formation. A layer-by-layer method was developed to construct titania-based inorganic/organic thin films on a range of substrates. A flow-based method in which aqueous solutions of papain, a wash buffer and TiBALDH were alternately flowed across a SiO_2 surface was employed. TiBALDH was selected as a mineral precursor because it undergoes very slow hydrolysis in aqueous solutions, and is regarded as a stable precursor for titania mineralization.[25] Successive mass deposition of enzyme or inorganic on the SiO_2 surface was assessed using quartz-crystal microbalance analysis with dissipation monitoring (QCM-D). QCM permits both the quantity and rate of material deposition to be monitored, with dissipation analysis (-D) providing a measure of the rigidity of the material deposited.[35] The role of the surface chemistry in thin-film formation was explored by comparing films formed on both bare SiO_2 and amine-terminated surfaces. This strategy was used with alternating flows of papain, wash buffer and TiBALDH to create either single or multi-layer papain-TiO_{2-x} composite thin-films in a highly controllable manner (Fig. 1).

The initial immobilization of papain on SiO_2 surfaces was rapid, as shown by a sharp drop in frequency (Δf) to -25 Hz in 30 seconds (Figs. 1a and 1b). This was followed by a slower adsorption phase (Figs. 1a and 1b, "Papain"), where deposition behavior was similar on both bare (Fig. 1a) and amine-modified SiO_2 surfaces (Fig. 1b). However, a larger overall frequency drop was observed for bare SiO_2 substrates across the two adsorption phases (to -45 Hz, Fig 1a "Papain"), where little of the slowly adsorbed papain was removed by washing. In contrast, papain adsorption on the amine-functionalized surface proceeded 10 times more slowly during the slow absorption phase, and was only partially removed with washing (Fig. 1b). The changes in dissipation are minor compared with the initial strong adsorption of papain to the SiO_2 surfaces (Figs. 1a and 1b). This suggests that the films formed on both surfaces are rigid,[35,36] which is consistent with published modelling studies.[30]

The total protein mass deposited on the amine-functionalized surface was calculated to be 0.44 µg cm^{-2}, which equates to 5.7 pmol cm^{-2} of papain (based on a film comprising 25 wt % water).[37] Taking the average diameter of papain to be 3.5 nm[38] the coverage on the amine-terminated surface is consistent with a close-packed monolayer of enzyme that covers 86% of available substrate surface area. The bare SiO_2 surface, in contrast, supported adsorption of 0.91 µg cm^{-2} papain, which is equivalent to ≈ 200 % surface coverage, suggesting enzyme multilayer formation. Papain binding to SiO_2 is dominated by electrostatic and van der Waals interactions between the protein's binding patch (see Figure S1) and the oxide surface.[30] However, papain can bind to surfaces in multiple

configurations[30] , which could give rise to an entirely different configuration on the SiO_2-amine surface. This is turn could promote multilayer packing on the bare SiO_2 surface compared with amine-modified SiO_2.

After removal of unbound enzyme, TiBALDH was flowed over the papain surface layers, resulting in the rapid formation of a composite inorganic/ organic film (Figs. 1a and 1b, "TiBALDH"; also see Fig. 2). The mineralization traces observed by QCM-D were qualitatively similar on both surfaces, but the total mass deposited was ≈1.5 times greater on the bare SiO_2-papain substrate than on the SiO_2-amine-papain surface. Dissipation changes revealed that while enzyme immobilized on the SiO_2-amine surface was capable of catalyzing the formation of a rigid mineralized film ($\Delta D < 1 \times 10^{-6}$), enzyme immobilized on bare SiO_2 surfaces catalyzed the formation of a softer film, as indicated by a change in ΔD of 5×10^{-6} over the mineralization frequency drop (Fig 1a, "TiBALDH").

This softer film could be related to diffusional constraints, such that the multilayer papain film on bare SiO_2 inhibits penetration of TiBALDH to the underlying enzyme layer. This is supported by measurements of the mass of titania deposed per enzyme; 981 ± 42.1 ng TiO_2/μg papain is deposited on the bare SiO_2 surface compared with 706 ± 39.4 Ti/μg papain on the SiO_2-amine surface. This suggests that the amine surface orients the protein on the surface, perhaps providing better exposure of the protein active site to solution. The deposition of titania is also a biphasic process, where 87% of the titania film was deposited on SiO_2-papain in the first 35 seconds, and the remaining 13% in the following 40 seconds (Fig S3). We suggest that the second, slower stage of mineral deposition is due to the diminishing access of Ti-BALDH to papain.

Previous studies have shown that TiO_2 mineralization from TiBALDH precursors can occur under basic conditions[39]. We therefore examined TiO_2 deposition directly on a SiO_2-amine surface (omitting an initial papain layer). TiO_2 deposition is indeed observed, as shown by a –12 Hz shift in frequency (Fig. 1c), equating to 216 ng cm^{-2} TiO_2, a process that does not occur on bare SiO_2 surfaces (Fig S2). However, this process took over 9-times longer than when papain was present, and the overall mineral mass deposition (as indicated by Δf) was ≈ 2-4 fold less than with the papain-mediated process.

Given that papain adsorbs to SiO_2 surfaces (Fig. 1a and 1b), and that TiO_2 is negatively charged at pH 7.0,[40] papain was also expected to adsorb to newly deposited TiO_{2-x} surfaces. This was confirmed by the data shown in Fig. 1d, which clearly demonstrates that papain readily deposits on titania films. This occurs to comparable degrees, and at a similar rate to that observed on SiO_2 surfaces (compare "Papain" in Fig. 1a with "P1" in Fig. 1d). Papain multilayers therefore form on the TiO_{2-x} films as they did on SiO_2 surfaces, and new papain layers also support deposition of TiO_{2-x} thin films when exposed to TiBALDH precursor (Fig. 1d, "T2" and "T3"), demonstrating that papain-directed thin film mineralization can be performed in a layer-by-layer process. Although the rates and total deposition

of papain-catalyzed TiO_{2-x} were similar for each individual layer, significant changes in dissipation were observed with the addition of each subsequent TiO_{2-x} layer. This suggests that after the initial deposition of a rigid film, subsequent layers are more loosely associated with the surface. This is manifested in the significant viscoelasticity of the multilayer composite structure (Fig. 1d, $\Delta D \sim 10 \times 10^{-6}$ after the final wash).

Morphological Analysis of Thin Films. Mineralized thin films were characterized using scanning electron microscopy (SEM) and energy dispersive spectroscopy (EDS) (Fig. 2), where samples were fractured and mounted to show the cross-section of the film. EDS analysis of a single-layer TiO_{2-x} film grown on a bare SiO_2 surface QCM chip (Fig. 2a; also see Fig. 1a) confirmed the presence of titanium (Fig. 2b). The thin film achieved *via* layer-by-layer deposition (Fig. 2c; also see Fig. 1d) was visibly thicker and rougher than the single-layer film, although both films were continuous in structure. SEM analysis of the thicknesses of films deposited on QCM-D crystals was challenging due to rupturing of the mineral layers during sample preparation. Films for SEM were therefore prepared using successive dip-coating on a glass microscope slide (alternating immersion of the slide in papain and TiBALDH solutions). Using this method, triple-layer films exhibited a film thickness of ~320 nm (Fig. 2d). As the papain surface layer is expected to be only ≈3-10 nm thick,[30] this suggests that the titania/ papain thin films form as a direct result of the enzymatic turnover of TiBALDH into a hydrolyzed titanium species which undergo mineralization as they diffuse away from the enzyme surface. This mechanism is supported by the finite thicknesses of the resulting titania films, demonstrating that film growth does not occur autocatalytically (i.e., this level of mineralization does not occur on titania surfaces without papain to act as a catalyst). Once the enzyme layer becomes passivated by titania, it creates a diffusional barrier that prevents further TiBALDH from reaching the surface-bound enzyme.

Analysis of Kinetics. To elucidate whether papain enzymatically catalyzes titania mineralization, we examined the kinetics of mineralization in bulk solution using *in situ* fluorescence. This was achieved by examining the spectral shift exhibited by a fluorescent coumarin dye (7-diethylaminocoumarin-3-carboxylate hydrazide) as it becomes incorporated into the thin films (Fig. S4). Analysis of papain-mediated TiO_2 formation in bulk solution phase revealed a similar mechanism to that occurring on the solid substrates, where the papain becomes passivated during mineralization and is unable to convert all available TiBALDH precursor into solid product (Fig. S5). The initial rate of deposition of TiO_2 on the substrate was linear (Fig. S6), allowing analysis of the kinetics of the early stages of mineralization (Fig. 3a).

Obtaining mineralization kinetics requires the dye fluorescence to be correlated with the mass of titania produced. This was achieved using a calibration curve that was constructed by preparing a range of papain-driven titania mineralization reactions in the presence of a fixed concentration of the reporter dye (Fig. S7). The papain concentration was increased across the reaction set, yielding increasing quantities of titania precipitates in a concentration-dependent manner. End-point fluorescence measurements were acquired, and the precipitates were washed using buffer replacement and successive centrifugation, before being dried and weighed. Finally, the measured masses were adjusted to account for the titania product only and the mass associated with co-precipitating lactate species was disregarded. This adjustment was enabled by thermogravimetric analysis (TGA), which showed that the precipitate is composed of ≈40% TiO_2 mineral and ≈60% organic (lactate) matter (Fig. S8). Therefore, the final calibration-curve relates fluorescence directly to the product titania (Fig. S7).

This curve was used to derive the kinetic plots shown in Fig. 3a, which fits reasonably well to a Michaelis-Menten model (R^2=0.95) as described in the native catalysis of papain[42]. However, a Hill plot kinetic model fits even better (R^2=0.99). This discrepancy between native activity and the best fit model is likely caused by the fact we are examining precipitates, and may reflect a 2-step process comprising the initial enzymatic step and a rapid non-enzymatic step. Michaelis-Menten modeling of the whole process revealed an apparent K_M of 0.45mM and k_{cat} of 1.26 1/sec (Fig. 3a). Slow kinetics of metal substrate hydrolysis have also been suggested to be important in the control of crystallization by biomineralizing enzymes.[20] Papain exhibits a range of specificity constants for peptide hydrolysis, varying from 10^3-10^6 $M^{-1}s^{-1}$ against varying polypeptide substrates, and k_{cat} values ranging from 0.24 s^{-1} to 34 s^{-1}.[44] The kinetic values we find here are therefore consistent with values reported for papain activity against polypeptide substrates *in vitro*.

Deactivated Papain does not Mineralize Titania. To further confirm that the mineralization process was enzyme-mediated, deactivation studies were conducted. Papain has a well-described catalytic triad (Cys25, His159 and Asn195) active site and previous studies have shown that deactivation of Cys25 results in a functionally inactive enzyme[41,42]. To inactivate the enzyme we took advantage of the accessible active site cleft of papain and modified Cys25 (Figure 3b) using maliamide-biotin covalent modification[43] as confirmed by western blot (Figure 3c). Modification of Cys25 with biotin resulted in a completely inactive enzyme, as shown by the lack of titania deposition activity by kinetics (Figure 3a) and lack of ability to drive titania deposition as monitored by QCM-D (Figure 3d). These two sets of evidence strongly suggest that the titania mineralization is enzymatically-driven. However, its

mechanism may be that it continuously catalyzes a titania species that then behaves as a nucleation species.

Characterization of TiO_2 Polymorph. Lastly, the mineral phases present in the multilayer papain-TiO_{2-x} films were characterized using Raman microscopy, synchrotron powder X-ray diffraction, and transmission electron microscopy (TEM) and selected area electron diffraction (SAED). Synchrotron powder XRD of powders produced by reaction of papain with TiBALDH in bulk solution showed that the enzymatically-synthesized mineral products comprise both anatase and rutile in a ratio of 3.5:1 (Fig. 4). Raman analysis of a film prepared on a glass slide by a simple dip-coating method revealed that it contained some crystalline titania. The film exhibited broad Raman peaks centered at 142 cm^{-1}, 395 cm^{-1}, 513 cm^{-1}, and 637 cm^{-1}, where these are in good agreement with those observed from an anatase TiO_2 reference powder (Fig. S9). As the peaks were broad, some overlap occurs with the signals expected from brookite or rutile (Fig. S9). However, annealing the film to 400 °C resulted in complete conversion to anatase (Fig. S9), supporting the Raman analysis. Additional characterization of both single layer (Fig. 5a) and multilayer (Fig. 5b) films was also conducted by TEM, where the films were directly deposited on formvar-covered Cu TEM grids via dip coating. EDS analysis confirmed the presence of Ti and O (Fig. 5c) while high resolution TEM and SAED revealed that the films contain crystalline anatase TiO_2 nanoparticles (~3-5 nm) (Fig. 5d). These results show that surface-bound enzymes have the potential for generating crystalline thin films of titania under aqueous conditions.

Discussion

The ability of papain to support the formation of partially crystalline titania thin films raises interesting questions about the mechanisms of its catalytic activity. Initial evidence of papain's enzymatic control over thin film mineralization is found in the increased deposition of TiO_{2-x} on the papain-coated SiO_2-amine surface versus the protein-free SiO_2-amine surface (Fig. 1). Polyamines[45] and small molecule amines[39] have previously been shown to play a role in mineral oxide formation *in vivo*[45] and *in vitro*,[46] where this has been attributed to the production of a local pH increase that initiates precursor hydrolysis and promotes TiO_2 deposition. We demonstrate that the faster film growth and thicker films achieved on the papain-coated surface can be attributed to enzymatic turnover, where this rapidly generates hydrolyzed titanium species for incorporation into the newly forming thin film, even relatively distal to the surface. In this scenario, hydrolyzed precursors are formed adjacent to the film under the action of the enzyme, prior to condensing on the substrate to form a dense thin film that progressively covers the enzyme. This mechanism is supported by papain's ability to promote the formation of a ≈107nm continuous inorganic film in each layer.

To our knowledge, the present report represents the first time that enzymatic mineralization has been harnessed for layer-by-layer synthesis of inorganic thin films *in vitro*. Kroger and Sandhage, *et al.*

used the protein protamine to guide layer-by-layer formation of titania thin films functionalized with organic components.[48,49] However; the mineralization step in those studies relies solely on the electrostatic (and not enzymatic) properties of protamine.[48] The mineral layers generated by protamine were very thin (~4 nm),[49] and were also amorphous, requiring annealing at 500 °C to induce TiO_2 crystallization.[48] In contrast, papain was employed here to generate mineral coatings at room temperature that were much thicker than the individual enzyme molecules and which contained crystalline anatase nanoparticles. One previous study also examined the use of the biomineralizing enzyme silicatein to form a silica film *in vitro,*[14] but a layer-by-layer process was not utilized and growth of the oxide film occurred over days. This suggests that the majority of the film growth was not enzyme-controlled but rather occurred *via* a slow autocatalytic process after an initial silica layer had deposited on the enzyme film.

A nascent body of work examining enzymatic mineralization suggests that the chemical nature and solution accessibility of an enzyme's active site is an important determinant of the enzyme's ability to direct mineralization.[15,29,47,50] This implies that, for biomineralization processes utilizing enzymes, active-site catalysis of a small-molecule metal-organic substrate drives mineral nucleation and growth. Despite this, no previous study has described enzymatic mineralization using conventional kinetic descriptors. In two cases, Michaelis-Menten parameters were reported for mineralizing enzymes.[51,52] However, the parameters reported did not directly describe mineral production, but rather small-molecule transformations that were indirectly related to mineralization (either hydrolysis of silicon-ester bonds,[51] or ammonia production by urease[52]). The Michaelis-Menten parameters reported here are based on monitoring the formation of TiO_{2-x} solid as the reaction product, and in this sense are the first reported direct kinetic descriptors for enzymatic mineralization. We have also identified that a critical active site residue, Cys25, is essential in the mineralization process.

The utility of directly measuring mineral formation is highlighted by comparing the k_{cat} and k_{cat}/k_m values obtained here for papain-directed titania mineralization with those from urease-directed titania mineralization.[52] Overall, the kinetic descriptors of both enzymes are similar (k_{cat} = 0.37 s^{-1} and k_{cat}/K_M = 1.37 x 10^3 $M^{-1}s^{-1}$ for urease, and k_{cat} = 1.26 s^{-1} and k_{cat}/K_M = 2.8 x 10^3 $M^{-1}s^{-1}$ for papain in this study). However, while we observe that papain-driven titania mineralization occurs rapidly (within seconds), urease-driven mineralization occurs over the course of hours.[52] This discrepancy likely arises from the fact that the urease-mediated process does not involve direct processing of the titanium precursor species, but rather relates to a gradual increase in solution pH with concomitant base-driven hydrolysis of TiBALDH, where this stems from the enzymatic production of ammonia. In contrast, papain-controlled mineralization likely involves hydrolysis of the precursor by direct action of the enzyme. Overall, these results suggest that selection of enzymes that exhibit different mineralization kinetics

provides a route by which the mineral film thickness can be tuned, and the enzyme optimized, a prospect that is worthy of study in future work.

Experimental

Full experimental details are provided in the Supporting Information. Briefly:

Quartz Crystal Microbalance with Dissipation. QCM-D experiments were conducted on a Q-sense E4 using either amine-functionalized SiO_2 or non-modified SiO_2 sensor crystals at 22°C with the flow rate held at 70 µl.min^{-1}. SiO_2 surface modification was performed by immersing the sensor in a solution of 3-aminopropyltriethoxysilane.[56] Data shown exhibiting changes of dissipation (ΔD) and frequency (Δ*f*) (Fig. 1) are shown from the 7th overtone for clarity. The cumulative data was used to model the viscoelastic properties of the adsorbed papain and the TiO_2 deposition. This modeling was conducted using QTools 2 QSense software under the assumptions of the Kevin-Voigt model,[57,58] a hydrodynamic protein density of 1200 k-gm^{-3} [37,59] and a TiO_2 nominal density of 4.23 kgm^{-3} The Sauerbrey equation was used to calculate the mass of the papain film:

Thin film formation *via* dip-coating: Layer-by-layer synthesis of titania thin films on glass substrates was conducted via a dip-coating process where glass substrates were immersed in a protein solution of 1 mM papain in 100 mM MES pH 7.0 for 30 s, followed by a wash immersion in distilled deionized water for 30 s, followed by a mineralization immersion in 20 mM TiBALDH for 5 min, followed by a second wash in distilled deionized water for 15 s. This cycle was repeated 3 times, after which the glass substrate was subject to two additional washes in ethanol and distilled deionized water for 15 s, respectively, and then air-dried. A similar process was used to deposit thin films on formvar-covered TEM grids.

Optical transmission measurements of enzymatic mineralization. Transmittance measurements were conducted using UV/VIS spectrometery. A 0.9 mL solution of 1 mM TiBALDH in 20 mM MES pH 7.0 was transferred to a quartz cuvette and at time t=0, 0.1 mL 20 µM papain in 20 mM MES pH 7.0 was added to the same cuvette. Transmittance was recorded at a constant wavelength of 650 nm in time-drive mode. After the precipitates settled to the bottom of the cuvette and the transmittance recovered, an additional dose of 0.1 mL 20 µM papain in 20 mM MES pH 7.0 was added to the cuvette.

Characterization via electron, fluorescence confocal, and Raman microscopies: The morphologies of the thin films deposited on glass slides were characterized using SEM, while nanostructure sand crystal phase were studied using TEM. Fluorescent probe (DCCH) incorporation into the layer-by-layer assembled films (Fig. S4) was confirmed using fluorescent confocal microscopy, while Raman microscopy was used to confirm polymorph.

Synchrotron Powder XRD Analysis. Enzymatic mineralization was conducted in 10 mL of a bulk solution reaction using 20 μM Papain and 1 mM TiBALDH in pH 7.0 20 mM MES. High-resolution X-ray powder diffraction measurements were carried out on the synchrotron beamline (I11) at Diamond Light Source (Didcot, UK).

Determination of papain enzyme mineralization kinetics. TiBALDH-papain enzyme kinetics for titania precipitation were derived from fluorescence emission increases (recorded at 590 nm); this emission increase served as a proxy for mineral precipitate formation (Figs. S4 and S6). Fluorescence measurements were made using a plate reader and assays were conducted in 96 well plates. Precipitation progress was tracked by sequential fluorescent measurements at 0.1 sec intervals (Ex: 405 nm, Em: 590 nm) at a constant temperature of 21°C. To relate fluorescence intensity to the quantity of titania mineral produced, the composition of the precipitate was first analyzed using thermogravimetric analysis (TGA) to infer the mass percent of mineral in the precipitate (e.g., Fig. S8). In this way, the measured fluorescence intensity was related to the millimoles of TiBALDH converted (Fig. S7), and this information was used to obtain enzyme kinetic parameters assuming Michaelis–Menten behavior. Only the onset values of precipitate formation were used for kinetic analysis.[61]

Conclusions

Papain's capacity for producing continuous titania films on a range of substrates *via* a simple dip coating approach suggests a widespread potential for adapting biomimetic mineralization strategies for the production of advanced materials. Mineralizing enzymes have been shown to generate a number of crystalline metal oxides from water-soluble precursors,[18] including SnO_2[53] and quartz-like silicates,[15] and to produce silver nanoparticles for sensing applications.[54] Such enzymes are also amenable to directed laboratory evolution of enhanced self-assembly and mineral synthesis activities,[15,55] where surface absorption, chemical catalysis, and mineral templating are all genetically tunable enzyme features that can be tailored towards the formation of thin film materials. The potential for re-engineering enzymes such as papain offers a route to controlling the properties of semiconductor thin films, where the layer-by-layer processing approach developed here provides additional control and could ultimately enable synthesis of crystalline heterostructures. Combined with kinetic descriptors to quantitatively assess enzymatic biomineralization activity, the approach described here should advance both the understanding and technological potential of biomimetic mineralization.

Conflicts of interest

There are no conflicts to declare.

Acknowledgements

This work was supported by an Engineering and Physical Sciences Research Council (EPSRC) Leadership Fellowship, EP/H005374/1 (F.C.M., L.A.B. and J.I.). D.G.G.M and L.J.C.J were supported by the UK Biotechnology and Biological Sciences Research Council and the Engineering and Physical Science Research Council (BB/G009228). L.A.B. and D.G.G.M. thank the EPSRC Directed Assembly Network for a seed fund grant that partially supported this work and D.G.G.M. also thanks the University of Delft (Startup grant). M.A.L. thanks the US-UK Fulbright Commission for a Fulbright Postgraduate Award. We also thank Diamond Light Source for access to Beamline I11 under proposal EE10425. We thank Chiu C. Tang of the Diamond Light Source for assistance with synchrotron powder XRD data acquisition, Dr Yi-Yeoun Kim (University of Leeds) for assistance with XRD analysis and Dr Alex Kulak (University of Leeds) for assistance with SEM.

References

1 D. T. Read, and A. A. Volinsky, in *Micro-and opto-electronic materials and structures: Physics, mechanics, design, reliability, packaging* (eds. Suhir, E., Lee, Y. C. & Wong, C. P.) **1,** A135–A180 (Springer, 2007).

2 M. M. Pendergast and E. M. V. Hoek, A review of water treatment membrane nanotechnologies. *Energy Environ. Sci.* 2011, **4**, 1946.

3 M. Grätzel, Recent Advances in Sensitized Mesoscopic Solar Cells. *Acc. Chem. Res.* 2009, **42**, 1788–1798.

4 T. P. Chou, *et al.* Organic–inorganic hybrid coatings for corrosion protection. *J. Non-Cryst. Solids.* 2001, **290**, 153–162.

5 J. H. Holtz and S. A. Asher, Polymerized colloidal crystal hydrogel films as intelligent chemical sensing materials. *Nature* 1997, **389**, 829–832.

6 P. T. Hammond, Form and Function in Multilayer Assembly: New Applications at the Nanoscale**. *Adv. Mater.* 2004, **16,** 1271.

7 K. L. Choy, Chemical vapour deposition of coatings. *Prog. Mater. Sci.* 2003, **48**, 57–170.

8 S. C. Tjong, and H. Chen, Nanocrystalline materials and coatings. *Mat. Sci. Eng. R-Rep.* 2004, **45**, 1–88.

9 S. C. Jain, M. Willander, J. Narayan, and R. V. Overstraeten, III–nitrides: Growth, characterization, and properties. *J. Appl. Phys.* 2000, **87**, 965.

10 M. I. Siponen, P. Legrand, M. Widdrat, S. R. Jones, W. Zhang, M. C. Y. Chang, D. Faivre, P. Arnoux, D. Pignol, Structural insight into magnetochrome-mediated magnetite biomineralization. *Nature* 2013, **502**, 681–684.

11 J. Aizenberg, J. C. Weaver, M.S. Thanawala, V. C. Sundar, D. E. Morse, P. Frazi, Skeleton of Euplectella sp.: structural hierarchy from the nanoscale to the macroscale. *Science* 2005, **309**, 275–278.

12 J. C. Weaver, G. W. Milliron, A. Miserez, K. Evans-Lutterodt, S. Herrera, I. Gallana, W. J. Mershon, B. Swanson, P. Zavattieri, E. DiMasi, D. Kisailus, The Stomatopod Dactyl Club: A Formidable Damage-Tolerant Biological Hammer. *Science* 2012, **336**, 1275–1280.

13 S. R. Whaley, D. S. English, E. L. Hu, P. F. Barbara, and A. M. Belcher, Selection of peptides with semiconductor binding specificity for directed nanocrystal assembly. *Nature* 2000, **405**, 665–668.

14 A. Polini, S. Pagliara, A. Camposeo, A. Biasco, H. C. Schroeder, W. E. G. Muller, D. Pisignano, Biosilica Electrically-Insulating Layers by Soft Lithography-Assisted Biomineralisation with Recombinant Silicatein. *Adv. Mater.* 2011, **23**, 4674–4678.

15 L. A. Bawazer, M. Izumi, D. Kolodin, J. R. Neilson, B. Schwenzer and D. E. Morse, Evolutionary selection of enzymatically synthesized semiconductors from biomimetic mineralization vesicles. *Proc. Natl. Acad. Sci. U.S.A.* 2012, **109**, E1705–E1714.

16 S. Mann, Biomineralization: Principles and Concepts in Bioinorganic Materials Chemistry. (Oxford University Press, 2001).

17 Y.-Y. Kim, K. Ganesan, P. Yang, A. N. Kulak, S. Borukhin, S. Pechook, L. Ribero, R. Kröger, S. J. Eichhorn, S. P. Armes, B. Pokroy, and F. C. Meldrum, An artificial biomineral formed by incorporation of copolymer micelles in calcite crystals. *Nat. Mater.* 2011, **10**, 890–896.

18 R. L. Brutchey, and D. E. Morse, Silicatein and the Translation of its Molecular Mechanism of Biosilicification into Low Temperature Nanomaterial Synthesis. *Chem. Rev.* 2008, **108**, 4915–4934.

19 K. M. Roth, Y. Zhou, W. Yang, and D. E. Morse, Bifunctional Small Molecules Are Biomimetic Catalysts for Silica Synthesis at Neutral pH. *J. Am. Chem. Soc.* 2005, **127**, 325–330.

20 L. A. Bawazer, J., Ihli, T. P. Comyn, K. Critchley, C. J. Empson, and F. C. Meldrum, Genetic Algorithm-Guided Discovery of Additive Combinations That Direct Quantum Dot Assembly. *Adv. Mater.* 2015, **27**, 223-227.

21 M. Sarikaya, C. Tamerler, A. K.-Y. Jen, K. Schulten, and F. Baneyx, Molecular biomimetics: nanotechnology through biology. *Nat. Mater.* 2003, **2**, 577–585.

22 P. Laaksonen, S. R. Szilvay, and M. B. Linder, Genetic engineering in biomimeticcomposites. *Trends. Biotechnol.* 2012, **30**, 191–197.

23 A. Rao, J. K. Berg, M. Kellermeier, and D. Gebauer, Sweet on biomineralization: effects of carbohydrates on the early stages of calcium carbonate crystallization. *Eur. J. Mineral.* 2014, **26**, 537–552.

24 K. Shimizu, J. Cha, G. D. Stucky, and D. E. Morse, Silicatein alpha: cathepsin L-like protein in sponge biosilica. *Proc. Natl. Acad. Sci. U.S.A.* 1998, **95**, 6234–6238.

25 J. L. Sumerel, W. J. Yang, D. Kisalius, J. C. Weaver, J. H. Choi, and D. E. Morse, Biocatalytically Templated Synthesis of Titanium Dioxide. *Chem. Mater.* 2003, **15**, 4804–4809.

26 P. Curnow, D. Kisailus, and D. E. Morse, Biocatalytic Synthesis of Poly(L-Lactide) by Native and Recombinant Forms of the Silicatein Enzymes. *Angew. Chem. Int. Ed.* 2006, **45**, 613–616.

27 H. Miyamoto, T. Miyashita, M. Okushima, S. Nakano, T. Morita, and A. A. Matsushiro, Carbonic anhydrase from the nacreous layer in oyster pearls. *Proc. Natl. Acad. Sci. U.S.A.* 1996, **93**, 9657–9660.

28 A. Ahmad, P. Mukerjee, D. Mandal, S. Senapati, M. I. Khan, R. Kumar, and M. Sastry, Enzyme Mediated Extracellular Synthesis of CdS Nanoparticles by the Fungus, *Fusarium oxysporum*. *J. Am. Chem. Soc.* 2002, **124**, 12108–12109.

29 G. P. Smith, K. J. Baustian, C. J. Ackerson, and D. L. Feldheim, Metal oxide formation by serine and cysteine proteases. *J. Mater. Chem.* 2009, **19**, 8299–8306.

30 J. He, M. Wu, X. Feng, X. Shao, and W. Cai, Immobilization of papain on nanoporous silica. *RSC Adv.* 2014, **4**, 13304–13312.

31 S. Solís, J. Paniagua, J. C. Martínez, and M. Asomoza, Immobilization of papain on mesoporous silica: pH effect. *J. Sol-Gel. Sci. Technol.* 2006, **37**, 125–127.

32 X. Wang, U. Schlossmacher, M. Wiens, R. Batel, H. C. Schröder, and W. E. G. Müller, Silicateins, silicatein interactors and cellular interplay in sponge skeletogenesis: formation of glass fiber-like spicules. *FEBS J.* 2012, **279**, 1721–1736.

33 C. Stremnitzer, K. Manzano-Szalai, A. Willensdorfer, P. Starkl, M. Pieper, P. König, M. Mildner, E. Tschachler, U. Reichart, and E. Jensen-Jarolim, Papain Degrades Tight Junction Proteins of Human Keratinocytes *In Vitro* and Sensitizes C57BL/6 Mice via the Skin Independent of its Enzymatic Activity or TLR4 Activation. *J. Invest. Dermatol.* 2015, **135**, 1790–1800.

34 P. Curnow, P. H. Bessette, D. Kisailus, M. M. Murr, P. S. Daugherty, and D. E. Morse, Enzymatic Synthesis of Layered Titanium Phosphates at Low Temperature and Neutral pH by Cell-Surface Display of Silicatein-α. *J. Am. Chem. Soc.* 2005, **127**, 15749–15755.

35 F. Höök, B. Kasemo, T. Nylander, C. Fant, K. Sott, and H. Elwing, Variations in Coupled Water, Viscoelastic Properties, and Film Thickness of a Mefp-1 Protein Film during Adsorption and Cross-Linking: A Quartz Crystal Microbalance with Dissipation Monitoring, Ellipsometry, and Surface Plasmon Resonance Study. *Anal. Chem.* 2001, **73**, 5796–5804.

36 F. Höök, M. Rodahl, P. Brzezinski, and B. Kasemo, Energy dissipation kinetics for protein and antibody-antigen adsorption under shear oscillation on a quartz crystal microbalance. *Langmuir* 1998, **14**, 729–734.

37 C. Zhou, J. M. Friedt, A. Angelova, K. H. Choi, W. Laureyn, F. Frederix, L. A. Francis, A. Campitelli, Y. Engelborghs, and G. Borghs, Human Immunoglobulin Adsorption Investigated by Means of Quartz Crystal Microbalance Dissipation, Atomic Force Microscopy, Surface Acoustic Wave, and Surface Plasmon Resonance Techniques. *Langmuir* 2004, **20**, 5870–5878.

38 R. Ménard, H. E. Khouri, C. Plouffe, R. Dupras, D. Ripoll, T. Vernet, D. C. Tessier, F. Laliberte, D. Y. Thomas, and A.C. Storer, A protein engineering study of the role of aspartate 158 in the catalytic mechanism of papain. *Biochemistry* 1990, **29**, 6706–6713.

39 T. Fröschl, U. Hörmann, P. Kubiak, G. Kucerova, M. Pfanzelt, C. K. Weiss, R. J. Behm, N. Hüsing, U. Kaiser, K. Landfester, and M. Wohlfahrt-Mehrens, High surface area crystalline titanium dioxide: potential and limits in electrochemical energy storage and catalysis. *Chem. Soc. Rev.* 2012, **41**, 5313.

40 S. Begonja, L. A. G. Rodenas, E. B. Borghi, and P. J. Morando, Adsorption of cysteine on TiO_2 at different pH values: Surface complexes characterization by FTIR-ATR and Langmuir isotherms analysis. *Colloids Surf, A.* 2012, **403**, 114–120.

41 I. G. Kamphuis, K. H. Kalk, M. B. Swarte, and J. Drenth, Structure of papain refined at 1.65 angstroms resolution. *J. Mol. Biol.* 1984, **179**, 233–256

42 G. Venturini, E. Fioravanti, M. Colasanti, T.Persichini, and P. Ascenzi, Cys25-Nitrosylation inactivates papain *Biochem. Mol. Biol. Intl.* 1998, **46**, 425–428.

43 D. G. G. McMillan, R. Watanabe, H. Ueno, G. M. Cook, and H. Noji, Biophysical characterization of a thermoalkaliphilic molecular motor with a high stepping-torque gives insight into evolutionary ATP synthase adaptation. *J. Biol. Chem.* 2016, **291***,* 23965–23977

44 C. Serveau, L. Juliano, P. Bernard, T. Moreau, R. Mayer, and F. Gauthier, New substrates of papain, based on the conserved sequence of natural inhibitors of the cystatin family. *Biochimie* 1994, **76**, 153–158.

45 N. Kröger, R. Deutzmann, and M. Sumper, Polycationic peptides from diatom biosilica that direct silica nanosphere formation. *Science* 1999, **286**, 1129–1132.

46 N. Kröger, M. B. Dickerson, G. Ahmad, Y. Cai, M. S. Haluska, K. H. Sandhage, N. Poulsen, and V. C. Sheppard, Bioenabled Synthesis of Rutile (TiO_2) at Ambient Temperature and Neutral pH. *Angew. Chem. Int. Ed.* 2006, **45**, 7239–7243.

47 J. C. Weaver, and D. E. Morse, Molecular biology of demosponge axial filaments and their roles in biosilicification. *Microsc. Res. Tech.* 2003, **62**, 356–367.

48 Y. Fang, Q. Wu, M. B. Dickerson, Y. Cai, S. Shian, J. D. Berrigan, N. Poulsen, N. Kröger, and K. H. Sandhage, Protein-Mediated Layer-by-Layer Syntheses of Freestanding Microscale Titania Structures with Biologically Assembled 3-D Morphologies. *Chem. Mater.* 2009, **21**, 5704–5710.

49 J. D. Berrigan, T. Kang, Y., Cai, J. R. Deneault, M. F. Durstock, and K. H. Sandhage, Protein-Enabled Layer-by-Layer Syntheses of Aligned, Porous-Wall, High-Aspect-Ratio TiO_2 Nanotube Arrays. *Adv. Funct. Mater.* 2011, **21**, 1693–1700.

50 M. B. Frampton, and P. M. Zelisko, A Comparison of Protease Active Sites and their Ability to Process Silicon-Based Substrates. *Silicon* 2011, **4**, 51–56.

51 W. E. G. Müller, U. Schlossmacher, C. Eckert, A. Krasko, A. Boreiko, H. Ushijima, S. E. Wolf, W. Trernel, I. M. Müller, and H. C. Schröder, Analysis of the axial filament in spicules of the

demosponge Geodia cydonium: Different silicatein composition in microscleres (asters) and megascleres (oxeas and triaenes). *Eur. J. Cell. Biol.* 2007, **86**, 473–487.

52 J. M. Johnson, N. Kinsinger, C. Sun, D. Li, and D. Kisailus, Urease-Mediated Room-Temperature Synthesis of Nanocrystalline Titanium Dioxide. *J. Am. Chem. Soc.* 2012, **134**, 13974–13977.

53 R. André, M. N. Tahir, H. C. C. Schröder, W. E. G. Müller, and W. Tremel, Enzymatic Synthesis and Surface Deposition of Tin Dioxide using Silicatein-α. *Chem. Mater.* 2011, **23**, 5358–5365.

54 L. Rodríguez-Lorenzo, R. de la Rica, R. A. Álvarez-Puebla, L. M., Liz-Marzán, and M. M. Stevens, Plasmonic nanosensors with inverse sensitivity by means of enzyme-guided crystal growth. *Nat. Mater.* 2012, **11**, 604–607.

55 L. A. Bawazer, From DNA to genetically evolved technology. *MRS Bull.* 2013, **38**, 509–518

56 N. Aissaoui, L. Bergaoui, J. Landoulsi, J-F. Lambert, and S. Boujday, Silane Layers on Silicon Surfaces: Mechanism of Interaction, Stability, and Influence on Protein Adsorption. *Langmuir* 2012, **28**, 656–665.

57 S. X. Liu, and J.-T. Kim, Application of Kevin–Voigt Model in Quantifying Whey Protein Adsorption on Polyethersulfone Using QCM-D. *J. Lab. Autom.* 2009, **14**, 213–220.

58 M. V. Voinova, M. Rodahl, M. Jonson, and B. Kasemo, Viscoelastic acoustic response of layered polymer films at fluid-solid interfaces: continuum mechanics approach. *Phys. Scripta* 1999, **59**, 391–396.

59 M. Rodahl, F. Höök, C. Fredriksson, C. A. Keller, A. Krozer, P. Brzezinski, M. Voinova, and B. Kasemo, Simultaneous frequency and dissipation factor QCM measurements of biomolecular adsorption and cell adhesion. *Faraday Discuss.* 1997, **107**, 229–246.

60 S. P. Thompson, J. E. Parker, J. Potter, T. P. Hill, A. Birt, T. M. Cobb, F. Yuan, and C. C. Tang, Beamline I11 at Diamond: A new instrument for high resolution powder diffraction. *Rev. Sci. Instrum.* 2009, **80**, 075107. doi: 10.1063/1.3167217.

61 K. A. Johnson, and R. S. Goody, The Original Michaelis Constant: Translation of the 1913 Michaelis–Menten Paper. *Biochemistry* 2011, **50**, 8264–8269.

62 C. S. Hanes, Studies on plant amylases: The effect of starch concentration upon the velocity of hydrolysis by the amylase of germinated barley. *Biochem. J.* 1932, **26**, 1406–1421.

63 U. K. Laemmli, Cleavage of structural proteins during the assembly of the head of bacteriophage T4. *Nature.* 1970 **227**, 680–685

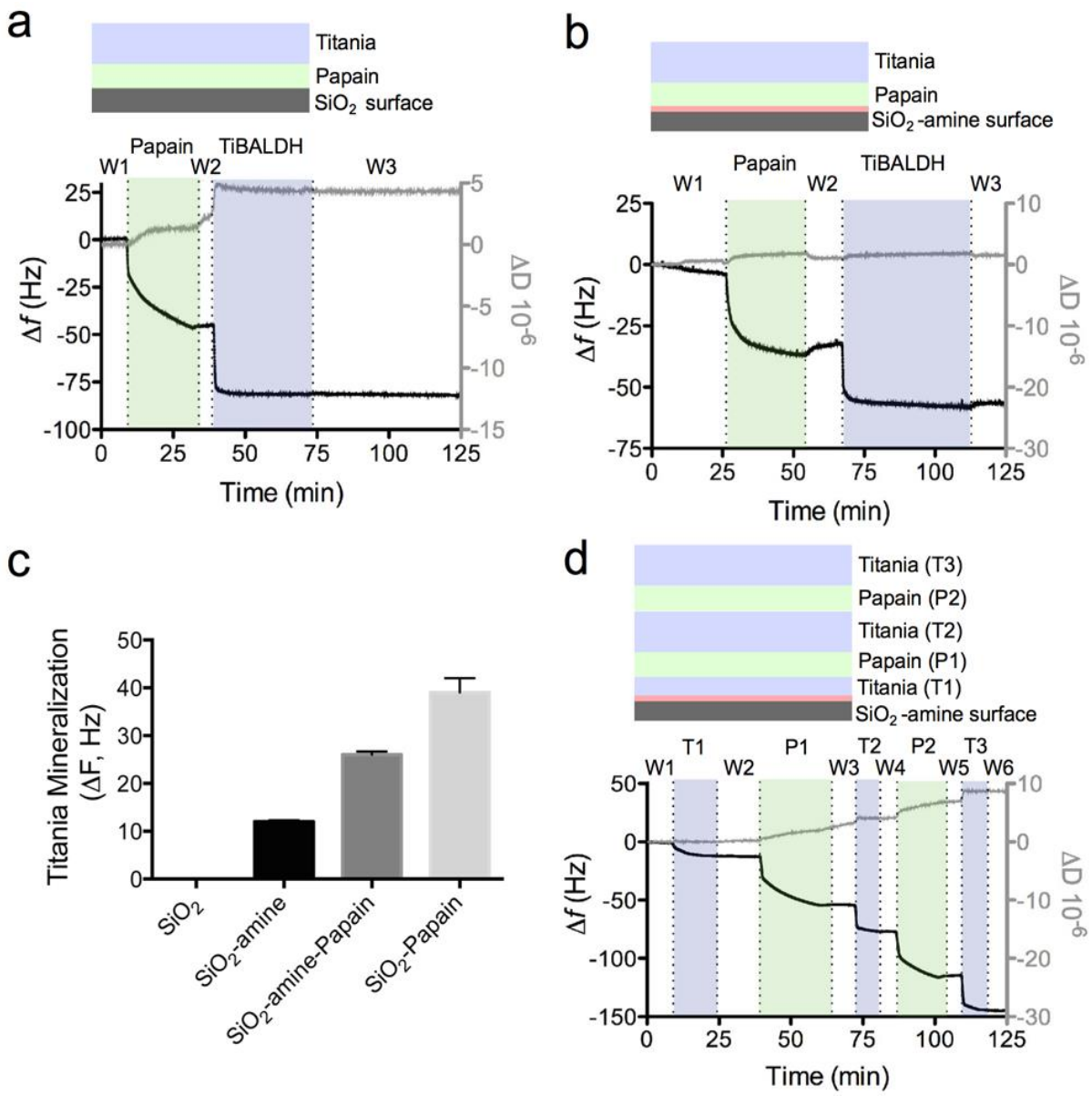

Figure 1. QCM-D analysis of papain-mediated titania thin film synthesis, where the associated schematics show the thin film structure. For QCM-D time-course plots (*a,b,d*), both frequency (black line, left axis) and dissipation (grey line, right axis) are shown, and changes in solution flows are indicated, where "W" indicates wash buffer (20 mM MES buffer pH 7.0), "Papain" indicates 10 µM papain in 20 mM MES buffer at pH 7.0, and "TiBALDH" represents 20 mM TiBALDH + 24 µM coumarin in water (pH 8.2). (a) Single-layer mineralized film synthesized on a bare SiO_2 surface. (b) Single-layer mineralized film synthesized on an amine-modified SiO_2 surface. (c) A comparison of the frequency changes which occur upon flow of TiBALDH over various surfaces, which serves as a proxy for the degree of titania mineralization. (d) Triple-layer mineralized film synthesized on an amine-modified SiO_2 surface. The plot shown are representative of triplicate experiments.

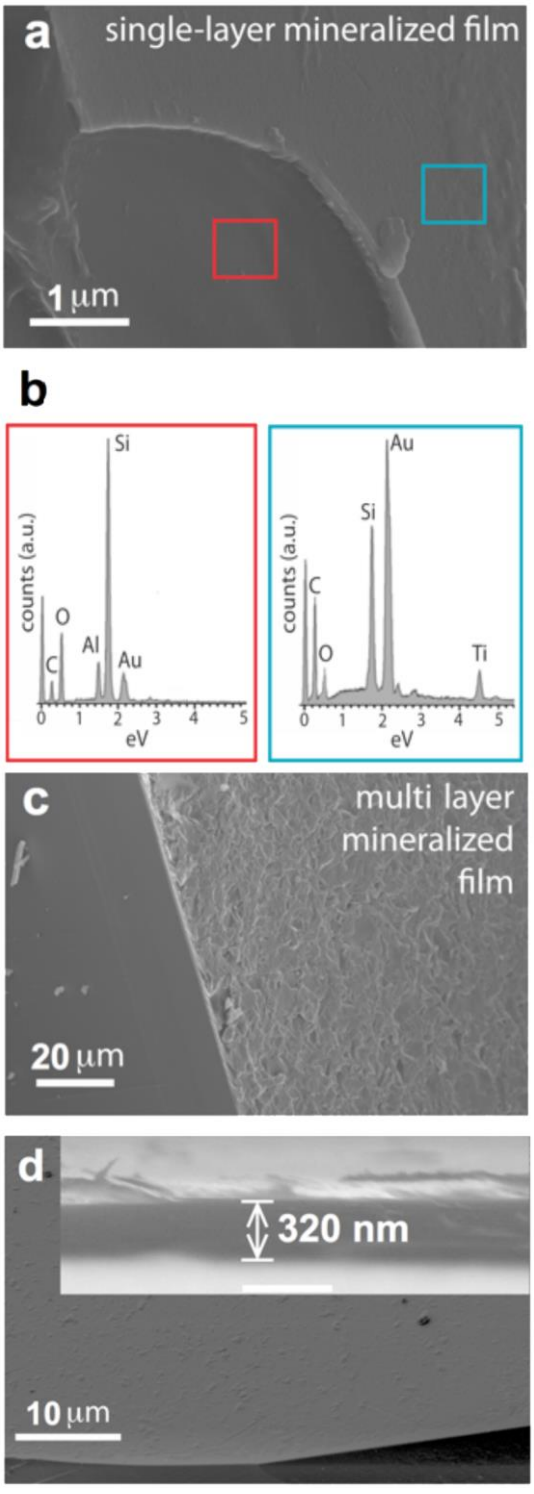

Figure 2. SEM and energy dispersive spectroscopy analysis (EDS) of papain/ titania thin films. Substrates supporting the mineralized films were fractured and imaged near the fracture edge. (a) SEM image of a single-layer film grown as summarized in Fig. 1a, on a quartz-gold-amorphous SiO_2 QCM surface. Red and blue boxes indicate surface areas analyzed by EDS. The red-boxed region is an area of exposed quartz substrate and the blue-boxed region is an area of stacked thin films, which

includes both the gold/amorphous SiO_2 layer of the commercial QCM-D substrate and the mineralized papain/TiO_{2-x} film. (b) EDS spectra confirm the presence of titanium in the papain-mineralized film region, where this is absent from the underlying quartz substrate. (c) SEM image of a multi-layer film, which was grown as in Fig. 1d. (d) SEM images of a triple-layer papain-titania film synthesized on a glass slide substrate. Imaging at a viewing angle of 45° (main image) shows the continuous nature of the mineralized film; the partial delamination of the film in the lower right of the image is a result of substrate fracture. Imaging at a viewing angle of 90° (inset) reveals a triple-layer titania film thickness of ca. 320 nm. The results shown are representative of triplicate experiments.

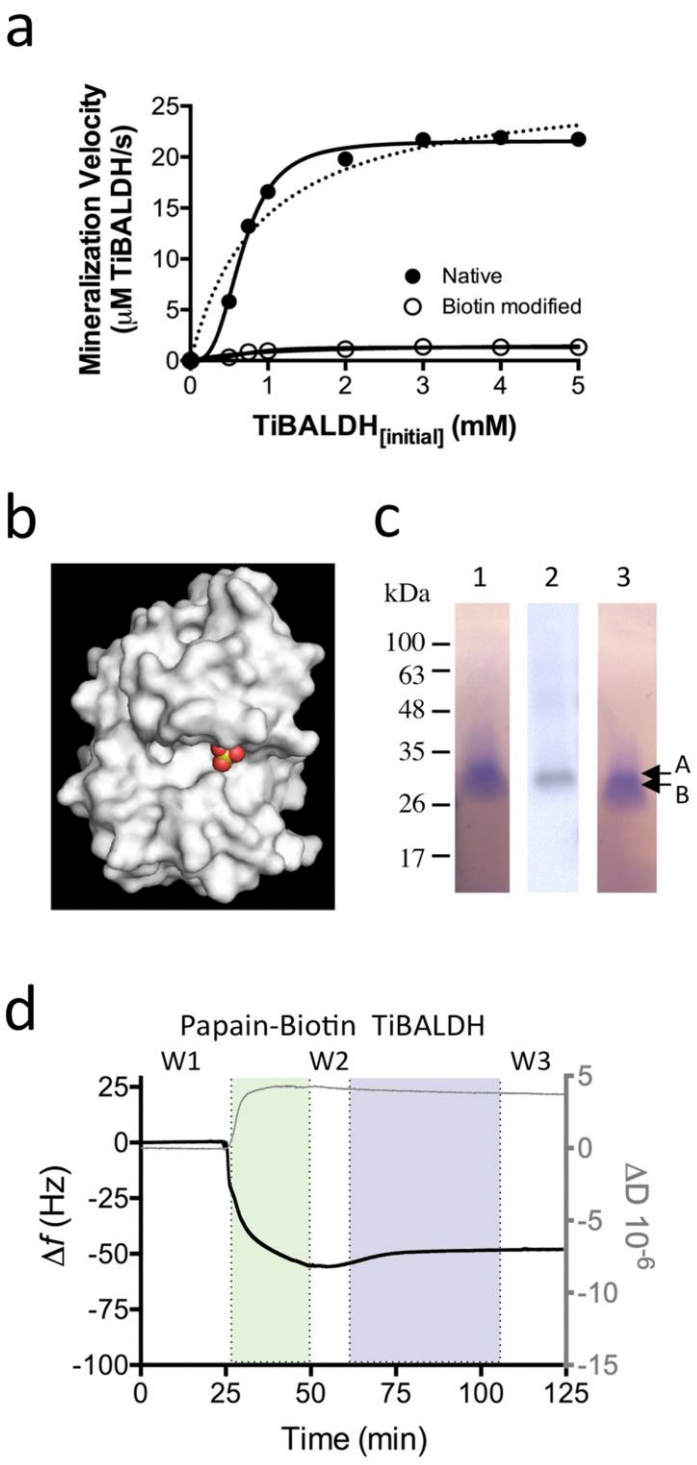

Figure 3. Kinetic analysis of papain-catalyzed TiO_2 synthesis in bulk solution using DCCH dye fluorescence as a proxy for titania mineralization (see Figs. S4 and S7). (a) Kinetic models of the initial rate of mineralization versus the concentration of mineral precursor (TiBALDH). WT papain data (filled circles) is shown fitted with a Michaelis-Menten model (dashed line; $R^2 = 0.95$), and a Hill equation (solid line; $R^2 = 0.99$). Inactivated (Cys25-biotin modified) papain is shown in open circles. The error is less than 5% and error bars shown. (b) A cartoon space-filling model showing the location of Cys25

(yellow and red spheres) in the active site cleft. The structure is 9PAP.pdb, published by Kamphuis *et al* (1984)[41] and this model was constructed and rendered using Pymol (Delano scientific). (c) *Lanes 1 and 3*, SDS-PAGE analysis of the purified, biotin-labeled papain (*Lane 1*) or papain (*Lane 3*) resolved using SDS-PAGE stained with Coomassie. *B. Lane 2*, Prior to Western blot analysis, biotin-labeled papain was separated by SDS-PAGE. Papain-biotin was subsequently transferred onto a polyvinylidene difluoride membrane and immunoblotted using a streptavidin-alkaline phosphatase (AP) conjugate (Roche) directed against biotin-modified papain. *A* indicates the size of papain-biotin; B indicates the size of papain. 10µg of protein was used in all separations. (d) QCM-D analysis of papain-mediated titania thin film synthesis. For QCM-D time-course plots (*a,b,d*), both frequency (black line, left axis) and dissipation (grey line, right axis) are shown, and changes in solution flows are indicated, where "W" indicates wash buffer (20 mM MES buffer pH 7.0), "Papain-biotin" indicates 10 µM papain-biotin in 20 mM MES buffer at pH 7.0, and "TiBALDH" represents 20 mM TiBALDH + 24 µM coumarin in water (pH 8.2). The result shown is representative of duplicate experiments.

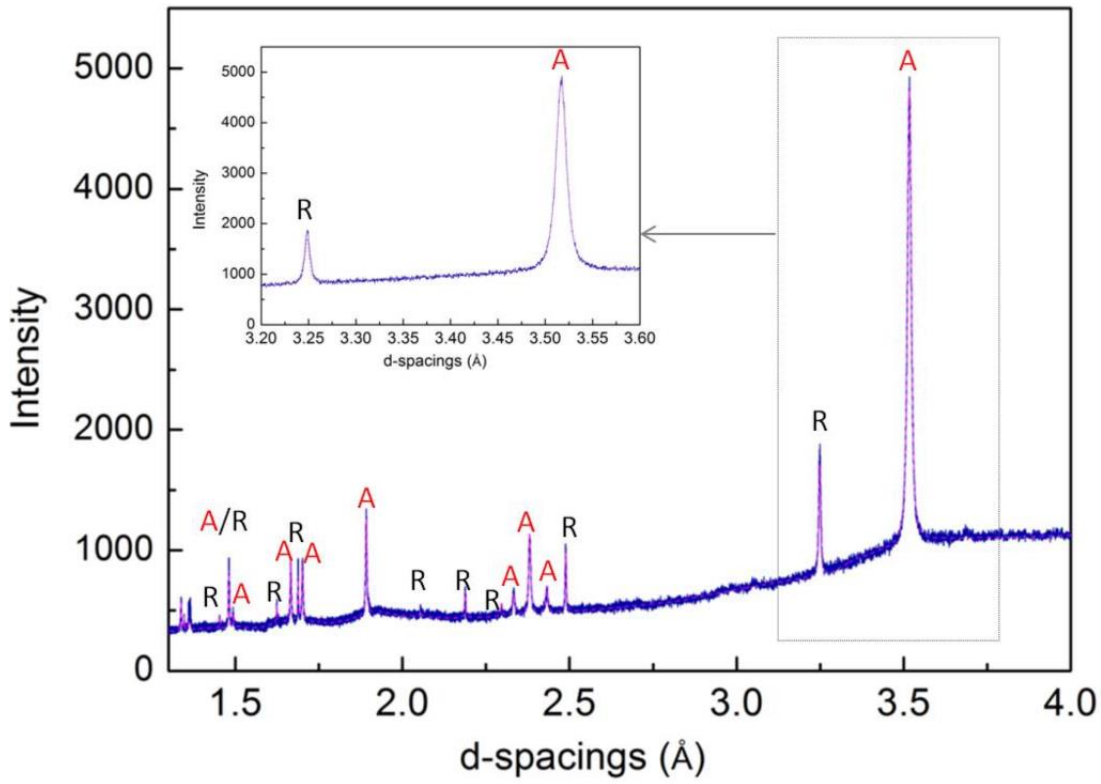

Figure 4. High-resolution synchrotron powder XRD spectra of titania precipitates generated from reaction of papain with TIBALDH (blue line) and fitting (pink dotted line). Peaks labelled A and R indicate the Anatase (COD 9015929) and Rutile (COD 9004144) phases of TiO_2, respectively (Anatase 93 %, Rutile 7 %).

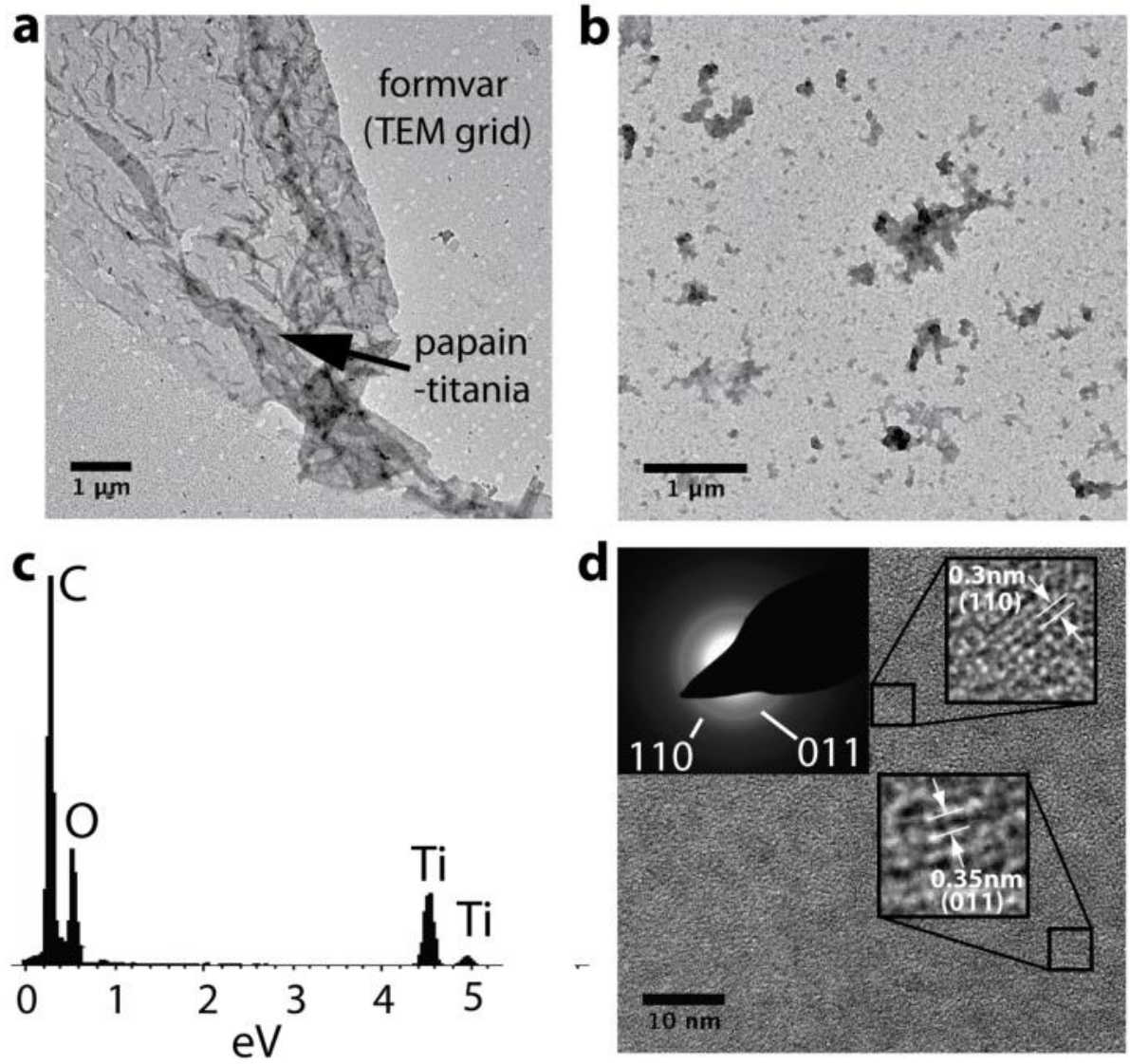

Figure 5. TEM analysis of papain-titania films mineralized on formvar-covered TEM grids *via* a dip-coating processing. (a) A single-layer titania film and (b) a 5-layer film. (c) EDS analysis from the film shown in (b). (d) Higher magnification TEM image of the film shown in (a), revealing inorganic nanoparticles within the film with crystalline lattice spacing that match well with the anatase (110) (top right inset) and (011) (bottom right inset) crystal planes, with corresponding SAED pattern (top left inset) confirming the presence of anatase.